

# Rydberg blockade with multivalent atoms: effect of Rydberg series perturbation on van der Waals interactions

Turker Topcu<sup>1,2,3</sup> and Andrei Derevianko<sup>1,2,3</sup>

<sup>1</sup>*Department of Physics, University of Nevada, Reno, Nevada 89557, USA*

<sup>2</sup>*ITAMP, Harvard-Smithsonian Center for Astrophysics, Cambridge, Massachusetts 02138, USA*

<sup>3</sup>*Physics Department, Harvard University, Cambridge, Massachusetts 02138, USA*

(Dated: October 19, 2021)

We investigate the effect of series perturbation on the second order dipole-dipole interactions between strontium atoms in  $5sns(^1S_0)$  and  $5snp(^1P_1)$  Rydberg states as a means of engineering long-range interactions between atoms in a way that gives an exceptional level of control over the strength and the sign of the interaction by changing  $n$ . We utilize experimentally available data to estimate the importance of perturber states at low  $n$ , and find that van der Waals interaction between two strontium atoms in the  $5snp(^1P_1)$  states shows strong peaks outside the usual hydrogenic  $n^{11}$  scaling. We identify this to be the result of the perturbation of  $5snd(^1D_2)$  intermediate states by the  $4d^2(^1D_2)$  and  $4dn's(^1D_2)$  states in the  $n < 20$  range. This demonstrates that divalent atoms in general present a unique advantage for creating substantially stronger or weaker interaction strengths than those can be achieved using alkali metal atoms due to their highly perturbed spectra that can persist up to high- $n$ .

PACS numbers: 32.80.Ee, 34.20.Cf, 37.10.Jk

## I. INTRODUCTION

Long-range interactions between Rydberg (Ry) atoms are useful in realizing conditional quantum dynamics, enabling a number of applications in quantum information processing (QIP) with neutral atoms [1–4]. Enabled by strong interactions between Ry atoms, the Rydberg blockade mechanism, which prohibits simultaneous excitation of two nearby Ry atoms, has particularly expanded the QIP toolbox. Applications of the Rydberg blockade include quantum logic gates [4, 5], simulation of exotic quantum many-body systems [6, 7], study of strongly-correlated systems [8, 9], and multiparticle entanglement generation [10]. Strong interactions between Rydberg states also facilitated the realization of strongly interacting individual photons paving the way for quantum non-linear optics at the single photon level [11, 12].

Most of the practical applications of Rydberg blockade have so far focused on alkali-metal atoms, *i.e.* atoms with a single valence electron outside a closed-shell core. Moving to multivalent atoms offers new possibilities in engineering quantum systems [13]. Divalent atoms, such as group-II atoms (*e.g.*, Mg, Ca, Sr) and group-II-like atoms such as Yb, Hg, Cd, and Zn are the simplest examples of multivalent atoms. Divalent atoms possess the advantage of an extra valence electron, which provides easier trapping with minimal loss and heating for Ry atoms trapped in a tight optical lattice [14, 15]. This is greatly beneficial as optical trapping is essential for QIP experiments due to the long coherence times that can be achieved. Coupled with mature experimental techniques for cooling and trapping divalent atoms [16–19], better trapping gives divalent atoms an edge over the alkali metal atoms in QIP and cold Rydberg experiments.

The most important long-range interaction between Ry atoms of the same parity is the second-order dipole-

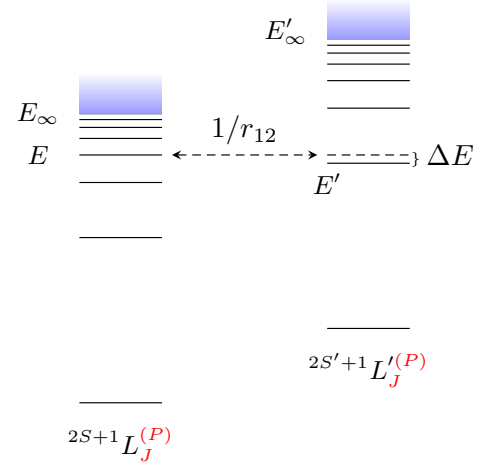


FIG. 1: (Color online) Illustration of series interaction where two Rydberg series  $2S+1 L_J^{(P)}$  and  $2S'+1 L'_J^{(P)}$  with the same total  $J$  and parity  $P$  converge to different ionization thresholds  $E_\infty$  and  $E'_\infty$ . If two states from these series happen to be close in energy (states labeled  $E$  and  $E'$ ), the Coulomb interaction  $1/r_{12}$  connecting these states can mix these states. The mixing is most prominent when the energy difference  $\Delta E$  is small compared to the Coulomb interaction matrix element.

dipole (or the van der Waals) interaction. Usually the van der Waals (vdW) interaction of alkali-metal atoms scales as  $n^{11}$ ,  $n$  being the principal quantum number of Ry states. Here we point out the substantial variations in this scaling law for multivalent atoms. This feature is unique for multivalent atoms as it caused by so-called Ry series interaction. For example, highly-excited energy levels of divalent atoms can be described by the electronic configuration  $n\ell n_r \ell_r$ . Then we may consider two Ry series  $n_1 \ell_1 n_r \ell_r$  and  $n_2 \ell_2 n'_r \ell'_r$  ( $n_1 \ell_1$  and  $n_2 \ell_2$  are

fixed, while  $n_r$  and  $n'_r$  are varied scanning through the series). Generally, such series exhibit the usual hydrogen-like behavior of energy levels. However, at some values of  $n_r$  and  $n'_r$  the energies of two series may come close to being degenerate (see Fig. 1). For such cases if the symmetries (the total angular momenta and parities) of the two series are identical, neither of the states remains a “good” eigenstate of the atomic Hamiltonian and the levels are mixed by the off-diagonal Coulomb interaction between configurations. This mechanism is well-known in spectroscopy [20] and is referred to as the series interaction or series perturbation.

As we demonstrate below the series interaction leads to substantial deviations from the  $n^{11}$  scaling law, with Ry states of the same series exhibiting both relatively small and large van der Waals interactions. The van der Waals interaction which depends on the interatomic separation  $R$  as  $C_6/R^6$  arises in the second-order in the dipole-dipole interaction between two Ry atoms. As any second-order contribution it is expressed as a sum over intermediate states with the energy denominator. The energy difference between the reference Ry+Ry states and intermediate diatom state, entering the denominator, can deviate from the nominal behavior due to the series interaction of the intermediate state with another series of the same symmetry. Namely this mechanism of intermediate state series perturbation is the cause of the irregularities in the van der Waals interaction strength. Such irregularities can be especially useful in asymmetric Ry blockade [13] which require simultaneous presence of both types of interaction strengths.

As a specific example we focus on Sr for its common use in optical lattice clocks and due the existence of well established experimental cooling and trapping techniques. We evaluate  $C_6$  coefficients for interactions between a pair of Sr atoms in  $5sns(^1S_0)$  and  $5snp(^1P_1)$  states. We show that the vdW interaction between two Sr atoms in  $5snp(^1P_1)$  states display highly non-monotonic behavior in the low- $n$  states ( $n \lesssim 20$ ), which does not lend itself to the smooth  $n^{11}$  scaling of the interaction strength. We trace the origin of this behavior to unusually small energy denominators in the second-order energy expression resulting from the strong variation in atomic energies due to the series interaction. In particular,  $nP+nP \rightarrow nD+(n-1)D$  channel contributes to the  $C_6$  coefficients with small energy denominators due to the highly perturbed nature of the  $5snd(^1D_2)$  series in Sr. Researching the literature, we find that the  $5snd(^1D_2)$  series is perturbed by the  $4d^2(^1D_2^e)$ ,  $5p^2(^1D_2^e)$  and  $4d6s(^1D_2^e)$  states, which lie below the ionization threshold of the  $5snd(^1D_2^e)$  series at  $45,932 \text{ cm}^{-1}$  [21]. Particularly, the  $4d6s(^1D_2^e)$  state perturbs states with  $n = 11 - 17$ ,  $5p^2(^1D_2^e)$  perturbs states with  $n = 5 - 6$  and  $4d^2(^1D_2^e)$  state perturbs the state with  $n = 12$  in the  $5snd(^1D_2^e)$  series. For the interaction between two Sr atoms in  $5sns(^1S_0)$  states, we do not see this non-monotonic behavior in the  $n$ -range we consider.

The paper is organized as follows: in the following section, we start with a brief description of the mech-

anism behind the series perturbation in divalent atoms in Sec. II. Then in Sec. III, we derive our formalism and describe the framework we work in. Results of our calculations follows in Sec. IV for the  $C_6$  coefficients corresponding to the  $^1S_0+^1S_0$  and  $^1P_1+^1P_1$  vdW interactions. Here we discuss the effects of the perturber states on the van der Waals interactions, which are pronounced for the  $5snp(^1P_1)$  Rydberg states with  $n \lesssim 20$ . In Sec. V, we calculate the angular dependence of the vdW interactions in terms of the contributions from different intermediate channels. Atomic units are used throughout this paper unless specifically stated otherwise.

## II. SERIES PERTURBATION IN DIVALENT ATOMS

We start by presenting a more detailed account of the series interaction mechanism and describe how it also results in second-order dipole-dipole interactions between divalent atoms that can strongly deviate from those between monovalent atoms, such as alkali metal atoms. Fig. 1 illustrates the basic physical picture. Two Rydberg series identified with the terms  $^{2S+1}L_J^{(P)}$  and  $^{2S'+1}L'_J{}^{(P')}$  have the same total angular momentum  $J$  and parity  $P$ . These series converge to different limits labeled as  $E_\infty$  and  $E'_\infty$ . Two levels  $E$  and  $E'$  in these series are very close in energy, which can be quantified by comparing the difference  $\Delta E$  to the off-diagonal matrix element of the Coulomb interaction evaluated between these states. Because of the accidental near degeneracy, the two levels repel each other, as long the corresponding matrix elements do not vanish. This is the reason why the two series must have the same  $J$  and  $P$ , as otherwise the Coulomb integral would vanish. In other words the character of the perturbing state (say  $E'$ ) is now mixed into the perturbed state  $E$ . Assuming that  $\Delta E$  is small enough, the Coulomb interaction shifts the total energy of the state up or down depending on the sign of the energy denominator. Typically, the Rydberg states lying above the perturbing state are shifted up in energy whereas the states below the perturbing state are shifted down [20].

The effect of series perturbation becomes more pronounced in high angular momentum states. Because the Rydberg electron is less influenced by the singly ionized core in higher angular momentum states, such as  $5snl$  states of Sr, these states are more hydrogenic in character. This increases the possibility of running into perturber states with close lying energies because the energies of the higher  $l$ -states start to become independent of  $l$  for a given  $n$  as in hydrogenic systems. This increases the density of states in a given energy interval, thereby increasing the number of states that are likely to be perturbed by a single perturber. For example, although the  $5sns(^1S_0)$  series of Sr is essentially unperturbed above  $n = 10$ , the  $5snd(^1D_2)$  series is substantially perturbed [21]. This can be seen from Fig. 2,

where we plot scaled energies  $En^{*2}$  for the  $5sns(^1S_0)$ ,  $5snp(^1P_1)$  and  $5snd(^1D_2)$  series of Sr. For Ry series that exhibit perfect hydrogenic energy scaling,  $En^{*2} = -1/2$  and the deviations from this value can be seen as a measure of how strongly the series is perturbed.

This feature of divalent atoms drastically affects the  $n$ -scaling of the van der Waals interaction. For two identical atoms in fixed magnetic sublevels, the expression for the vdW interaction reads

$$\delta E_{\text{vdW}} = \sum_{j,k} \frac{|\langle \psi(\text{I}) | \langle \psi(\text{II}) | V_{DD} | \phi_j(\text{I}) \rangle | \phi_k(\text{II}) \rangle|^2}{2E_\psi - (E_j + E_k)}. \quad (1)$$

In this work, the target states  $|\psi(\text{I}, \text{II})\rangle$  are  $|5sns(^1S_0)\rangle$  and  $|5snp(^1P_1)\rangle$ , where I and II refer to the two Sr atoms. The intermediate states  $|\phi\rangle$  run through the  $|5sn'p(^1P_1)\rangle$  states for the  $|5sns(^1S_0)\rangle$  target states, and they run through  $|5sn's(^1S_0)\rangle$ ,  $|5sn'd(^1D_2)\rangle$  and  $(|5sn's(^1S_0)\rangle + |5sn'd(^1D_2)\rangle)/\sqrt{2}$  for the  $|5snp(^1P_1)\rangle$  target states. The dipole-dipole interaction  $V_{DD}$  between two atoms (I and II) separated by a distance  $R$  is given by

$$V_{DD} = -\frac{1}{R^3} \sum_{\mu} w_{\mu}^{(1)} D_{\mu}^{(1)}(\text{I}) D_{-\mu}^{(1)}(\text{II}), \quad (2)$$

where  $w_{\mu}^{(1)} = 1 + \delta_{\mu,0}$  and the dipole operators are defined through their components as

$$D_{\mu}^{(1)} = -|e| \sum_k r_k C_{\mu}^{(1)}(\hat{\mathbf{r}}_k). \quad (3)$$

Here  $C_{\mu}^{(L)}(\hat{\mathbf{r}}) = \sqrt{4\pi/(2L+1)} Y_{\mu}^{(L)}(\hat{\mathbf{r}})$  are the normalized spherical harmonics where  $L$  runs over atomic electrons when the quantization axis is along the internuclear axis.

The expression (1) sensitively depends on energy denominators, thereby accidental near-degeneracies between target and the intermediate states can result in strong deviations from the hydrogenic scaling behavior of the long-range interaction strengths. We observe such effect in the van der Waals interactions between two  $5snp(^1P_1)$  Rydberg states of Sr, as this interaction has  $5snp(^1P_1) + 5snp(^1P_1) \rightarrow 5sn'd(^1D_2) + 5sn'd(^1D_2)$  as an intermediate channel where the  $5snd(^1D_2)$  states are highly perturbed below  $n \simeq 20$ .

To highlight the effect of series perturbation in the most clear fashion, we evaluate the vdW coefficients  $C_6$  for a non-degenerate manifold of magnetic substates. Zeeman degeneracy can be lifted by an application of external B-field and working with atoms trapped in a pancake-shaped cloud, so that the interactions occur in the pancake plane (internuclear axes for all diatoms lie in that plane). This trapping geometry is ubiquitous in practical realizations of optical lattice clocks [22–24] which are commonly carried out in 1D optical lattices. An external magnetic field  $\mathbf{B}$  is applied along the lattice axis, making the quantization axis orthogonal to  $\mathbf{R}$ , the internuclear separation. For a sufficiently strong magnetic field, we may neglect the vdW-induced mixing of

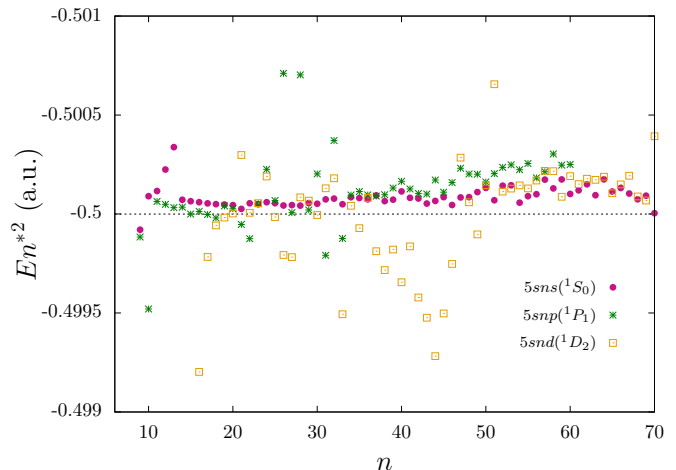


FIG. 2: (Color online) Scaled energies  $En^{*2}$  for the  $5sns(^1S_0)$ ,  $5snp(^1P_1)$  and  $5snd(^1D_2)$  series of Sr. It is clear that for higher  $J$  the energies fluctuate more and the deviation from the hydrogenic value  $-0.5$  a.u. is more pronounced.

magnetic sublevels and focus on a single  $M_B$  sublevel, with  $M_B$  being the projection of the atomic angular momentum along the B-field. The quantization axis in Eq. (1) is along the interatomic axis  $\hat{\mathbf{R}}$ . We rotate the dipole operator  $V_{DD}$  from  $\hat{\mathbf{R}}$  to the direction of the B-field by rotating  $D_{\mu}^{(1)}$  in Eq. (2) by angle  $\theta$  with respect to the pancake plane. Rotation by an angle  $\theta$  can be achieved by a set of rotations defined by the Euler angles  $\alpha = 0$ ,  $\beta = \theta$  and  $\gamma = 0$ . If we denote the rotation operator by  $\hat{S}$ , the normalized spherical harmonics in Eq. (3) transform as

$$C_{M_K}^{(K)}(\hat{S}\hat{\mathbf{r}}) = \sum_{M=-K}^K C_M^{(K)}(\hat{\mathbf{r}}) \mathbb{D}_{M,M_K}^{(K)}(0, \theta, 0), \quad (4)$$

where  $\mathbb{D}_{M,M'}^{(K)}(\alpha, \theta, \gamma)$  are the Wigner  $D$ -functions [25]. This results in the rotated dipole operator

$$D_{\mu}^{(1)}(\hat{S}\hat{\mathbf{r}}) = -\sum_j r_j \sum_{M=-1}^1 C_M^{(1)}(\hat{\mathbf{r}}_j) \mathbb{D}_{M,\mu}^{(1)}(0, \theta, 0). \quad (5)$$

Notation  $M_x$  in the text denotes the specific case of  $\theta = \pi/2$  when the B-field is pointing along the laser propagation axis. We perform our numerical calculations for this case and then extend the analysis to an arbitrary angle.

### III. VAN DER WAALS INTERACTIONS

Now we focus on evaluating the second order dipole-dipole (or the van der Waals) interaction between two identical Rydberg atoms. Because it is second order in the dipole-dipole interaction, vdW interaction scales as

$1/R^6$  with inter-atomic separation and corresponds to the  $-C_6/R^6$  term in the conventional multipole expansion of the long-range interactions. We are interested in the interactions between two  $5sns(^1S_0)$  and two  $5snp(^1P_1)$  state atoms. When evaluating the interaction between  $5snp(^1P_{1,M_B})$  and  $5snp(^1P_{1,M'_B})$  states, we will only be considering the stretched  $M_B = 1$  and  $M'_B = 1$  state. For two spherically-symmetric  $5sns(^1S_0)$  atoms the rotation of quantization axis is irrelevant and  $M_B = M \equiv 0$ .

Explicit derivation of the vdW interaction expressions in the LS coupling is given in the Appendix. The vdW interaction for two Sr atoms in  $5sns(^1S_0)$  Rydberg states can be expressed as

$$C_6(5sns(^1S_0)(\text{I})5sns(^1S_0)(\text{II})) = -\frac{2}{3} \sum_{n_2, n'_2} \frac{|\langle ns || d || n_2 p \rangle|^2 |\langle ns || d || n'_2 p \rangle|^2}{2E_{ns} - (E_{n_2 p} + E_{n'_2 p})}, \quad (6)$$

where  $d$  are the atomic dipole moment operators. The  $n_2 p$  and  $n'_2 p$  states reflect the electronic configurations of the intermediate dimer states  $|5sn_2 p(^1P_1)\rangle_{\text{I}} |5sn'_2 p(^1P_1)\rangle_{\text{II}}$ . Because we work in the LS coupling scheme, the contributions from  $^3P_1$  intermediate states are ignored because they contribute through spin-changing transitions, which are forbidden in the non-relativistic formalism and therefore are suppressed.

For the interaction between two  $5snp(^1P_1)$  atoms in the  $M_x = M'_x = 1$  magnetic substates,

$$C_6(5snp(^1P_{1,1_x})(\text{I})5snp(^1P_{1,1_x})(\text{II})) = \frac{1}{36} S_{ss} + \frac{181}{3600} S_{dd} + \frac{11}{72} S_{sd}. \quad (7)$$

The structure of this expression reflects two possible single-atom dipole excitation channels  $5snp(^1P_1) \rightarrow 5sn_2 s(^1S_0)$  and  $5snp(^1P_1) \rightarrow 5sn_2 d(^1D_2)$  with the reduced sums  $S$

$$S_{ss} = - \sum_{n_2, n'_2} \frac{|\langle np || d^{(1)} || n_2 s \rangle|^2 |\langle np || d^{(1)} || n'_2 s \rangle|^2}{2E_{np} - (E_{n_2 s} + E_{n'_2 s})},$$

$$S_{dd} = - \sum_{n_2, n'_2} \frac{|\langle np || d^{(1)} || n_2 d \rangle|^2 |\langle np || d^{(1)} || n'_2 d \rangle|^2}{2E_{np} - (E_{n_2 d} + E_{n'_2 d})},$$

$$S_{sd} = - \sum_{n_2, n'_2} \frac{|\langle np || d^{(1)} || n_2 s \rangle|^2 |\langle np || d^{(1)} || n'_2 d \rangle|^2}{2E_{np} - (E_{n_2 s} + E_{n'_2 d})}.$$

While computing the one-electron reduced matrix elements of the dipole operator, we use the three-parameter model potential of Ref. [26]:

$$U_l(r) = Be^{-Cr} - \frac{1 + (Z-1)e^{-Ar}}{r} + \frac{l(l+1)}{2r^2}. \quad (9)$$

In Ref. [26] the parameters of this model potential was obtained by fitting its eigenspectrum to experimental

data [27, 28] to minimize the differences between numerical and experimental energies for various terms such as  $^1S_0$ ,  $^1P_1$ ,  $^1D_2$ . Such fit is not adequate for our goals, as we need accurate energy denominators entering the second order dipole-dipole expression. Rather than fitting the energies from the model potential to experimental energies, we need to fit the energy denominators from the model potential to the experimental energy denominators. The potential quoted in Ref. [26] yields differences between the numerical and experimental energies that are comparable to the experimental energy denominators. Therefore we have modified some of the parameters in [26] to match the experimental energy denominators at high- $n$  ( $n \gtrsim 30$ ) and the new set of parameters are listed in Table I. The parameters marked with asterisks are those that are modified from the ones tabulated in Ref. [26].

The eigenenergy spectrum of the model potential (9) is smooth and it cannot reproduce the perturbed energy levels. To take the perturbed nature of the Ry series into account, we also evaluate the  $C_6$  coefficients using experimental energies in the denominator of Eq. (6) and (7). This gives us an *upper limit* for the fluctuations in  $C_6$  as we do not perform CI to determine our target and intermediate states. In the next section, we proceed to numerical evaluation of the vdW coefficients.

TABLE I: Parameters of the model potential (9) for the Rydberg electron in the  $5sns(^1S_0)$ ,  $5snp(^1P_1)$  and  $5snd(^1D_2)$  states of strontium. Most of the parameters are from Ref. [26], except the ones marked with asterisks, which were determined in this work by minimizing the differences between the experimental and the numerical values of energy denominators in the second order  $^1S_0 + ^1S_0$  (top) and  $^1P_1 + ^1P_1$  (bottom) van der Waals interactions.

	$5sns(^1S_0) + 5sns(^1S_0)$		
	A	B	C
$^1S_0$	3.762	-6.33	1.07
$^1P_1$	2.84*	-1.86	1.10
$^1D_2$	2.78	-9.06	2.31
	$5snp(^1P_1) + 5snp(^1P_1)$		
	A	B	C
$^1S_0$	5.599*	-6.33	1.07
$^1P_1$	3.49	-1.86	1.10
$^1D_2$	2.588*	-9.06	2.31

#### IV. RESULTS

Because the numerator of  $\delta E_{\text{vdW}}$  is proportional to the fourth power of the dipole operator ( $\propto n^8$ ) and the energy denominator scales as  $1/n^3$  for large  $n$ , the  $C_6$  coefficient is expected to scale as  $n^{11}$ . Although this behavior is exact for hydrogen, non-hydrogenic systems deviate from this scaling law: the softer the atomic core the more deviation from the  $n^{11}$  scaling law there is. Here, we report scaled  $C_6$  coefficients, *i.e.*  $\tilde{C}_6 = C_6/n^{11}$  so that any residual  $n$ -dependence leftover in  $\tilde{C}_6$  is atom dependent. The scaled  $\tilde{C}_6 = C_6/n^{11}$  coefficients for the van der Waals interaction between pairs of  $5sns(^1S_0)$  and  $5snp(^1P_{1,1_x})$  states are plotted as a function of  $n$  in the upper and lower panels of Fig. 3.

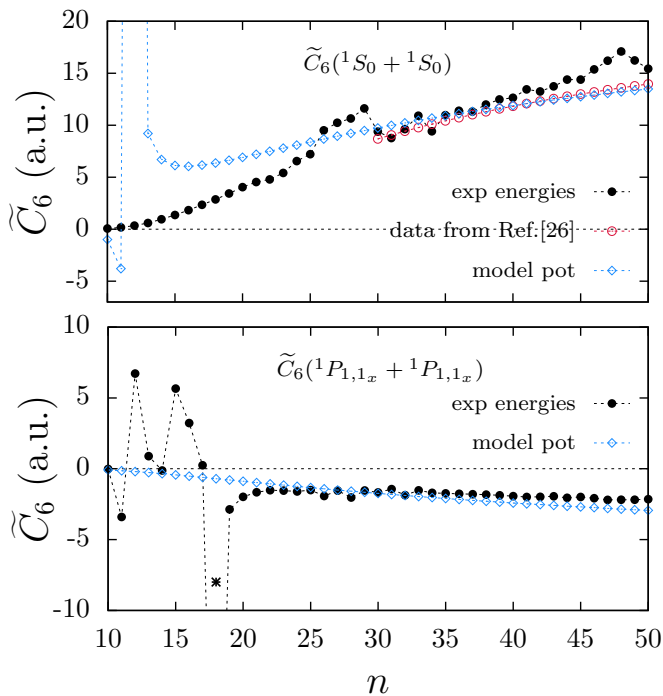


FIG. 3: (Color online) (Upper panel) Residual  $n$ -dependence of the  $C_6$  coefficients ( $\tilde{C}_6 = C_6/n^{11}$ ) for the  $5sns(^1S_0) + 5sns(^1S_0)$  van der Waals interaction in Sr. The blue open diamonds are calculated using the model potential quoted in the text. These match the data from Ref. [29] (red open circles) in the high- $n$  region. Replacing numerical energies from the model potential in the energy denominator with experimental energies results in solid black points. The positive  $\tilde{C}_6$  coefficients imply attractive interaction. (Bottom panel) Similar to the upper panel except for the  $5snp(^1P_{1,1_x}) + 5snp(^1P_{1,1_x})$  interaction. The blue open diamonds are evaluated using matrix elements and energies obtained from the model potential and solid black points using experimental energies in the energy denominator. The black star denotes the data point for  $n = 18$  outside the plot range.  $\tilde{C}_6(n = 18) \simeq -37$  a.u.

In the upper panel of Fig. 3, open blue diamonds show the  $\tilde{C}_6$  coefficients calculated using Eq. (6) in which both

the energies in the denominator and the one-electron orbitals in the reduced matrix elements are calculated using the model potential (9). The parameters in this model potential are adjusted from those listed in Ref. [26] to match the experimental energy denominators. This curve matches the data reported in Ref. [29] well (open red circles) for all  $n$  quoted in [29]. However, around  $n \approx 12$ , the  $\tilde{C}_6$  coefficients become extremely large due to almost vanishing energy denominator. Keeping in mind that the energies used in generating this set of  $\tilde{C}_6$  were calculated from the model potential (9), we find that the fitted potential has the pathological behavior at these low- $n$  such that the energy denominator flips sign going from  $n = 12$  to 11. This results in the unphysical resonance-like peak at  $n = 12$ . A side effect of this is to overestimate the  $\tilde{C}_6$  coefficients around  $n \lesssim 20$  due to the large contribution from  $n = 12$  intermediate state to the  $\tilde{C}_6$  coefficients of the nearby states. On the other hand, replacing the numerically calculated energies in the denominator of (6) by experimental values [27, 28, 30] results in the solid black points, which while matching the other two sets of data well at high  $n$ , keeps monotonically decreasing for  $n$  below 20 in accordance with the  $n^{11}$  scaling.

Unlike the  $5sns(^1S_0) + 5sns(^1S_0)$  interaction, numerically calculated values of  $\tilde{C}_6$  using the model potential (9) between  $5snp(^1P_{1,1_x})$  states do not display this pathological behavior at low- $n$  (open blue diamonds in the lower panel of Fig. 3). Replacing the numerically calculated energies in the denominators of Eq. (7) with experimental ones listed in [27, 28, 30] changes the  $\tilde{C}_6$  coefficients very little for  $n \gtrsim 20$  (solid black points).

We observe an unusual feature in the low- $n$  region below  $n = 20$ : the  $\tilde{C}_6$  coefficients display a non-monotonic behavior. Unlike the unphysical peak at  $n = 12$  in the  $^1S_0 + ^1S_0$  interaction, which stems from inaccurate representation of the soft-core potential at small distances, the non-monotonic features in the  $^1P_{1,1_x} + ^1P_{1,1_x}$  are etched in energy denominators derived from experimental spectra. For example, in the interaction between two  $5s18p(^1P_{1,1_x})$  states, the energy denominator in Eq.(7) involving the  $5s18p(^1P_{1,1_x})$ ,  $5s16d(^1D_2)$  and  $5s18d(^1D_2)$  states becomes unusually small, which gives the large peak at  $n = 18$ . The behavior of the energy denominator in the  $nP + nP \rightarrow n'D + n''D$  channel can be seen in Fig. 4. In order to emphasize its non-monotonic nature, we have plotted the scaled energy denominator  $1/(n^{*3}\Delta E)$  rather than  $\Delta E$ , where  $\Delta E$  is the energy difference  $2E_{nP} - (E_{n'D} + E_{n''D})$  and  $n^*$  is the effective principal quantum number. Notice that the energy denominators associated with the channels  $nP + nP \rightarrow (n-1)D + (n-1)D$  and  $nP + nP \rightarrow nD + nD$  are well behaved throughout all  $n$  (open green diamonds and open blue squares). This is to be expected from a hydrogen-like spectrum where the nearest-neighbor energy spacing sales as  $1/n^3$  for all  $n$ . On the other hand, whereas  $1/(n^{*3}\Delta E)$  is flat above  $n \sim 20$ , it is far from regular below  $n \sim 20$  in the channel  $nP + nP \rightarrow$



$nD + (n-1)D$ . Particularly at  $n = 18$ , the energy difference  $2E_{nP} - (E_{nD} + E_{(n-1)D})$  is unusually small resulting in the large peak. Besides being flat above  $n \sim 20$ ,  $1/(n^{*3}\Delta E)$  is also much smaller than the values at the peaks below  $n \sim 20$ , which translates into large  $\tilde{C}_6$  coefficients for the van der Waals interactions between  $^1P_{1,1_x}$  states in the region  $n \lesssim 20$ . It is also worth noting here that the open data points for  $\tilde{C}_6$  in Fig. 3 obtained using experimental energies represent an upper limit for  $\tilde{C}_6$ . This is because although the energy denominators in Eq. (7) are experimental, the matrix elements in the numerator do not include configuration interaction.

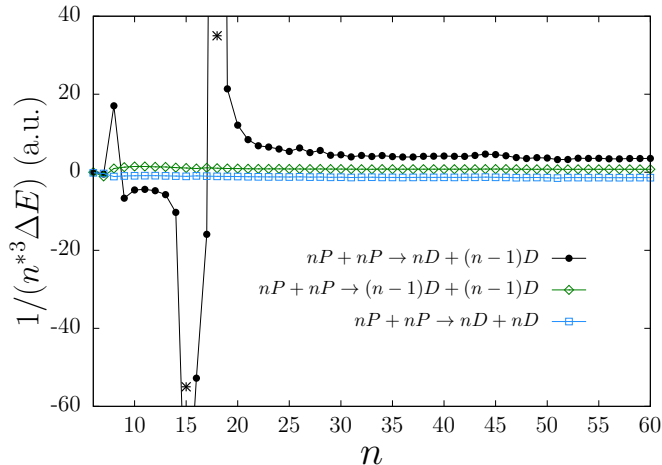


FIG. 4: (Color online) The scaled energy denominator in the second order perturbation theory expression for the  $\tilde{C}_6$  coefficients in the long range interaction between two  $5snp(^1P_{1,1_x})$  Sr atoms.  $\Delta E$  scales as  $1/n^{*3}$  as expected for the  $nP + nP \rightarrow (n-1)D + (n-1)D$  and  $nP + nP \rightarrow nD + nD$  interaction channels over the entire  $n$ -range. For the  $nP + nP \rightarrow nD + (n-1)D$  channel, however, this scaling breaks down for  $n \lesssim 20$  and  $1/(n^{*3}\Delta E)$  attain large values and changes sign. This “resonance-like” structure is facilitated by an unusually small  $\Delta E$  around  $n \sim 17$  and is possible because of the highly perturbed nature of the  $5snd(^1D_2)$  series in Sr.

The deviation of the nearest-neighbor energy differences from the hydrogenic  $1/n^3$  scaling is a consequence of the series perturbation. The scaled energies of the  $nS$ ,  $nP$  and  $nD$  Rydberg series are displayed as an inset in Fig. 4. Note that the energies of the  $5sns(^1S_0)$  states almost perfectly scale as  $1/n^{*2}$  for all  $n$ , whereas  $5snp(^1P_1)$  and  $5snd(^1D_2)$  states increasingly deviate from this scaling. This is because the states with higher angular momenta are more prone to being perturbed by other series. For a Rydberg series to be perturbed by another state, the perturber state needs to be below the ionization threshold for the Rydberg series in energy. Furthermore, it needs to have the same  $J$  and the parity for the associated Coulomb integral to be non-zero. Researching the literature, we have found that the  $5snd(^1D_2)$  series of Sr is perturbed by the  $4d^2(^1D_2^e)$ ,  $5p_{3/2}^2(^1D_2^e)$  and  $4d6s(^1D_2^e)$

states, all of which lie below the ionization threshold of the  $5snd(^1D_2^e)$  series at  $45,932 \text{ cm}^{-1}$  [21]. Other candidates with higher angular momenta that could perturb the  $5snd(^1D_2^e)$  series are  $4dng(^1D_2^e)$ , however, we could not find experimental data to confirm that these states actually lay below  $45,932 \text{ cm}^{-1}$ . We find that the  $4d6s(^1D_2^e)$  state perturbs states with  $n = 11 - 17$ ,  $5p^2(^1D_2^e)$  perturbs states with  $n = 5 - 6$  and  $4d^2(^1D_2^e)$  state perturbs the state with  $n = 12$  in the  $5snd(^1D_2^e)$  series. A detailed analysis of the  $5sns(^1S_0)$ ,  $5snp(^1P_1)$  and  $5snd(^1D_2)$  series and their perturbers is given in [21]. In contrast with the  $5snp(^1P_{1,1_x}) + 5snp(^1P_{1,1_x})$  interaction, we see no contribution from perturber states for the  $5sns(^1S_0) + 5sns(^1S_0)$  interaction at low- $n$  due to lower angular momentum of the perturber states in the  $^1S_0$  series [21].

Keeping in mind practical applications, we fitted the  $\tilde{C}_6$  coefficients to the same functions as the  $\tilde{C}_3$  and  $\tilde{C}_5$  coefficients and the fits parameters are listed in Table II. It is common practice is to fit these data to second or third degree polynomials [29]. One problem with this choice of fitting functions is that they can display wildly different behavior outside the fitted range of  $n$  and they diverge as  $n \rightarrow \infty$ . To evade this problem, we fit our data to functions which approach a fixed value as  $n \rightarrow \infty$ . In particular, we choose  $(an + b)/(n + d)$  and  $(an^2 + bn + c)/(n^2 + en + f)$  where  $a, b, c, d, e$  and  $f$  are fitting parameters. In the high- $n$  limit, both these functions approach  $a$ . Notice that these are smooth functions and cannot reproduce the non-monotonic behavior seen in Fig. 3. Results of our least-squares fitting for the  $\tilde{C}_3$  coefficients are tabulated in Table II. Parameters in Table II indicate in the limit  $n \rightarrow \infty$  the van der Waals interactions between pairs of  $5sns(^1S_0)$  atoms is roughly a factor of 3 stronger than those between pairs of  $5snp(^1P_{1,1_x})$  atoms. On the other hand, it is clear from Fig. 3 that picking  $n = 18$  results in much stronger van der Waals interactions between the  $5snp(^1P_{1,1_x})$  states than what would be expected from the fits quoted in Table II.

## V. ANGULAR DEPENDENCE

The dependence of the  $\tilde{C}_6$  coefficients for the  $^1P_{1,1_x} + ^1P_{1,1_x}$  van der Waals interaction on the angle  $\theta$  that the magnetic field makes with the internuclear axis can be expressed in term of the Legendre polynomials  $P_0(\cos\theta)$ ,  $P_2(\cos\theta)$  and  $P_4(\cos\theta)$ . The angular part of the interaction energy  $\delta E_{\text{vdW}}$  (A1) is contained in the square-

TABLE II: Fit parameters for the scaled  $\tilde{C}_6$  for fits of the form  $(an + b)/(n + d)$  and  $(an^2 + bn + c)/(n^2 + en + f)$  for the  $^1S_0 + ^1S_0$  and  $^1P_1 + ^1P_1$  van der Waals interactions. The  $\chi^2$  parameter for the lower order fit is  $\lesssim 0.05$  and  $\chi^2 < 10^{-4}$  in the higher order fit. One needs to go to  $n = 200$  for the difference between the two fits for the  $\tilde{C}_6$  coefficients to become  $\sim 10\%$ .

	$(an + b)/(n + d)$		
	$a$	$b$	$d$
$\tilde{C}_6(^1S_0 + ^1S_0)$	27.268	-116.556	41.926
$\tilde{C}_6(^1P_{1,1x} + ^1P_{1,1x})$	-11.036	112.5	97.176

	$(an^2 + bn + c)/(n^2 + en + f)$				
	$a$	$b$	$c$	$e$	$f$
$\tilde{C}_6(^1S_0 + ^1S_0)$	22.821	-473.021	3136.018	6.791	-129.797
$\tilde{C}_6(^1P_{1,1x} + ^1P_{1,1x})$	-6.342	97.465	-390.021	22.228	260.072

bracketed terms in Eq. (A4) and can be written as

$$\begin{aligned}
 f_{ss}(\theta) &= \frac{1}{45} + \frac{2}{63}P_2(\cos\theta) + \frac{2}{35}P_4(\cos\theta) \\
 f_{dd}(\theta) &= \frac{271}{4500} + \frac{32}{1575}P_2(\cos\theta) + \frac{1}{1750}P_4(\cos\theta) \\
 f_{sd}(\theta) &= \frac{23}{225} - \frac{1}{630}P_2(\cos\theta) + \frac{1}{175}P_4(\cos\theta),
 \end{aligned}$$

for the three channels involved, where we have denoted the angular part in Eq. (A4) with the function  $f$  (see Eq. (A6) in the Appendix).

The contributions from these three channels to the angular distribution of the coefficients  $|\tilde{C}_6|$  for three  $n$  values are plotted in Fig. 5. The  $nP + nP \rightarrow n'S + n''S$  channel contribution is depicted by the blue dotted curves, the  $nP + nP \rightarrow n'D + n''D$  channel by the red dashed and the  $nP + nP \rightarrow n'S + n''D$  channel by the brown dot-dashed curves. The total is plotted as the solid green curve in each case. It is clear from Eqs. (10) and Fig. 5 that the  $nP + nP \rightarrow n'S + n''S$  channel is dominated by  $P_4(\cos\theta)$  whereas the  $nP + nP \rightarrow n'D + n''D$  channel is dominated by  $P_2(\cos\theta)$ . All three channels contribute comparably to the total  $\tilde{C}_6$  over the range of all angles for  $n = 30$  and 50 which are states in the unperturbed part the Rydberg series with  $\tilde{C}_6$  behaving monotonically in Fig. 3. For  $n = 18$  however, the total  $\tilde{C}_6$  is entirely determined by the  $nP + nP \rightarrow n'D + n''D$  channel. This is because the resonance-like peak at  $n = 18$  in the bottom panel of Fig. 3 is due to the highly perturbed nature of the  $5snd(^1D_2)$  Rydberg series which result in an unusually small energy denominator for  $n = 18$  in the  $nP + nP \rightarrow n'D + n''D$  channel. The results we quote in the bottom panel of Fig. 3 and in Table II are for  $\theta = \pi/2$  which corresponds to the middle peak in the solid green curves in Fig. 5.

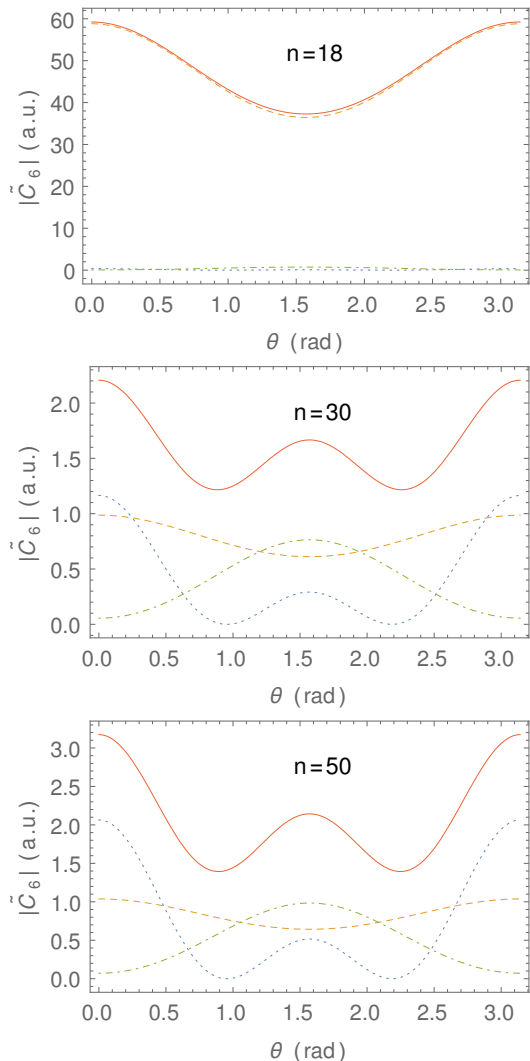


FIG. 5: (Color online) Angular distributions of the  $|\tilde{C}_6|$  coefficients for the van der Waals interaction between two  $5snp(^1P_{1,1x})$  Sr atoms (solid green curves) for various  $n$ , and the contributions to it from different intermediate channels:  $5sns(^1S_0) + 5sn's(^1S_0)$  (blue dotted),  $5snd(^1D_2) + 5sn'd(^1D_2)$  (dashed red), and  $5sns(^1S_0) + 5sn'd(^1D_2)$  (dotted dash brown). Note that the  $5sns(^1S_0) + 5sn's(^1S_0)$  channel is dominated by  $P_4(\cos\theta)$  whereas the  $5snd(^1D_2) + 5sn'd(^1D_2)$  channel is dominated by  $P_2(\cos\theta)$ . It is clear from the top panel that  $\tilde{C}_6$  is entirely determined by the  $P_2(\cos\theta)$  character of the  $5snd(^1D_2) + 5s(n-1)d(^1D_2)$  channel at  $n = 18$ , where the  $5snd(^1D_2)$  series is strongly perturbed.

## VI. CONCLUSION

Motivated by the recent interest in using divalent Rydberg atoms in quantum information processing we have calculated the van der Waals coefficients for two interacting Sr atoms in  $5sns(^1S_0)$  and  $5snp(^1P_1)$  Rydberg states.

We then calculate the  $C_6$  coefficients for the van der Waals interactions between two  $5sns(^1S_0)$  and two

$5snp(^1P_{1,M_x=1})$  Sr atoms. We find that our results are in good agreement with previously reported values in Ref. [29], which tabulated these  $C_6$  coefficients for  $n \geq 30$ . We also find that for  $n < 20$ , the scaled  $\tilde{C}_6$  coefficients describing the van der Waals interaction between two  $5snp(^1P_1)$  states show strong non-monotonic deviations from the hydrogenic  $1/n^{11}$  scaling due to the highly perturbed nature of the  $5snd(^1D_2)$  series as discussed in Ref. [21], which results in small energy denominators in the second-order expressions for the energy shifts. As a result, the  $\tilde{C}_6$  coefficients display highly non-monotonic behavior and change sign in the small  $n$ -region suggesting that the interaction can be made attractive or repulsive by choosing appropriate  $n$ . Particularly at  $n = 18$ ,  $\tilde{C}_6$  is much larger than any other state in the entire  $n$ -range we consider, which provides a possibility for engineering strongly asymmetric long-range interactions by contrast-

ing it with the van der Waals interaction between two Sr atoms in  $5sns(^1S_0)$  states.

## VII. ACKNOWLEDGEMENTS

This work was supported by the National Science Foundation (NSF) Grant No. PHY-1212482. A.D. was also supported by the Simons foundation as a Simons fellow in theoretical physics. T.T. and A.D. would like to thank the Institute for Theoretical Atomic, Molecular and Optical Physics (ITAMP) and the Harvard University Physics Department for their hospitality, where a part of this work was carried out. The authors would like to thank P. Kómár and M. D. Lukin for valuable discussions.

### Appendix A: Derivation of van der Waals expressions

Here we derive an expression for the van der Waals interaction energy correction for a pair of atoms,  $\delta E_{\text{vdW}}$ . The sets of quantum numbers of the two atoms (I and II) in the  $LSJ$  coupling scheme will be denoted as  $\gamma_1[L_1S_1J_1]_{M_1}$  (I) and  $\gamma'_1[L'_1S'_1J'_1]_{M'_1}$  (II), where the set of quantum numbers  $nl$  are denoted by  $\gamma$ . In particular we are interested in the van der Waals interactions between (1) two  $5sns(^1S_0)$  atoms with  $M_B = M'_B = 0$ , and (2)  $5snp(^1P_{1,M})$  and  $5snp(^1P_{1,M'})$  atoms with  $M_B = M'_B = 1$ .

The second order energy shift is given by

$$\delta E_{\text{vdW}}(\gamma_1[L_1S_1J_1]_{M_1}(\text{I})\gamma'_1[L'_1S'_1J'_1]_{M'_1}(\text{II})) = \frac{1}{R^6} \times \sum_{\substack{\gamma_2, \gamma'_2 \\ J_2, J'_2 \\ M_2, M'_2}} \frac{\left| \langle \gamma_1[L_1S_1J_1]_{M_1}(\text{I})\gamma'_1[L'_1S'_1J'_1]_{M'_1}(\text{II}) | V_{DD} | \gamma_2[L_2S_2J_2]_{M_2}(\text{I})\gamma'_2[L'_2S'_2J'_2]_{M'_2}(\text{II}) \rangle \right|^2}{(E_{\gamma_1[L_1S_1J_1]} + E_{\gamma'_1[L'_1S'_1J'_1]}) - (E_{\gamma_2[L_2S_2J_2]} + E_{\gamma'_2[L'_2S'_2J'_2]})}, \quad (\text{A1})$$

where  $V_{DD}$  is the rotated dipole-dipole interaction and the summation is over the intermediate states  $|\gamma_2[L_2S_2J_2]_{M_2}; \gamma'_2[L'_2S'_2J'_2]_{M'_2}\rangle$ . Because we are interested in the van der Waals interaction between atoms in identical electronic configurations, we take  $n_1 = n'_1 \equiv n_r$  and  $l_1 = l'_1 \equiv l_r$ .

To express the two-electron reduced matrix elements in terms of one-electron orbitals, we first transform the matrix element  $\langle ^1S_0 || D || ^1P_1 \rangle$  from the  $LSJ$  to the  $LS$  coupling,

$$\langle \gamma_1[L_1S_1J_1] || D || \gamma_2[L_2S_2J_2] \rangle = (-1)^{L_1+S_2+J_2+1} \sqrt{[J_1][J_2]} \begin{Bmatrix} L_1 & J_1 & S_2 \\ J_2 & L_2 & 1 \end{Bmatrix} \langle \gamma_1 L_1 || D || \gamma_2 L_2 \rangle \delta_{S_1, S_2}. \quad (\text{A2})$$

In the independent-particle approximation, the two-electron matrix element can be expressed in terms of a reduced matrix element involving only the single electron orbitals (see Ref. [31] for details). Since we are only interested in the singlet states  $S_1 = S_2 = 0$  and we obtain

$$\langle 5sn\ell(L_1) || D || 5sn'\ell'(L_2) \rangle = \sqrt{[L_1][L_2]} (-1)^{\ell'+L_1+1} \begin{Bmatrix} 1 & L_2 & L_1 \\ 0 & \ell & \ell' \end{Bmatrix} \langle n\ell || d || n'\ell' \rangle. \quad (\text{A3})$$

Here  $d$  is the one-particle dipole operator and  $D = \sum_{k=1}^2 d_k$  where the sum goes over the two atomic valence electrons. We also assume that the overlap between the  $n\ell$  state of the Rydberg electron and the  $5s$  state of the valence electron is negligible, which allows us to drop a second term involving  $\langle 5s || d || n'\ell' \rangle$  on the right hand side of Eq. (A3). Since Eq. (A3) now involves only the reduced matrix element for the Rydberg electron, we have removed the summation



over the valence electrons and dropped the index of  $d_k$ . Finally, we obtain

$$\begin{aligned} \delta E_{\text{vdW}}([L_1 S_1 J_1]_{M_1}(\text{I}) [L'_1 S'_1 J'_1]_{M'_1}(\text{II})) &= \frac{1}{R^6} \sum_{\substack{l_2, l'_2 \\ J_2, J'_2}} \\ &\left[ \sum_{\substack{M_1, M'_1 \\ M_2, M'_2}} \sigma_\theta(J_1, J'_1, M_1, M'_1; J_2, J'_2, M_2, M'_2) \sigma_\theta(J_2, J'_2, M_2, M'_2; J_1, J'_1, M_1, M'_1) \right] \\ &\times \left[ A(L_1, S_1, J_1, l_1; L_2, S_2, J_2, l_2) A(L'_2, S'_2, J'_2, l'_2; L'_1, S'_1, J'_1, l'_1) \right]^2 \\ &\times \sum_{n_2, n'_2} \frac{|\langle n_r l_r || d || n l_2 \rangle|^2 |\langle n_r l_r || d || n' l'_2 \rangle|^2}{(E_{L_1 S_1 J_1} + E_{L'_1 S'_1 J'_1}) - (E_{L_2 S_2 J_2} + E_{L'_2 S'_2 J'_2})}. \end{aligned} \quad (\text{A4})$$

Here we have factored out the summation over the magnetic quantum numbers which depends on the rotation angle of the quantization axis. The function  $\sigma_\theta$  describes the rotation of the quantization axis with respect to the inter-atomic axis, and the function  $A$  involves the factors from breaking up the two-electron reduced matrix elements into reduced one-electron matrix elements in the LS coupling scheme. Explicitly, these functions are given by

$$\begin{aligned} \sigma_\theta(J_1, J'_1, M_1, M'_1; J_2, J'_2, M_2, M'_2) &= \sum_{\mu} w_{\mu}^{(1)} (-1)^{M_1+M'_1} d_{M_1-M_2, \mu}^{(1)}(\theta) d_{M'_2-M'_1, -\mu}^{(1)}(\theta) \\ &\times \begin{pmatrix} J_1 & 1 & J_2 \\ -M_1 & M_1 - M_2 & M_2 \end{pmatrix} \begin{pmatrix} J'_1 & 1 & J'_2 \\ -M'_1 & -(M'_2 - M'_1) & M'_2 \end{pmatrix} \\ A(L_1, S_1, J_1, l_1; L_2, S_2, J_2, l_2) &= (-1)^{L_1+S_2+J_2+l_2+J_1} \sqrt{[J_1][L_1][J_2][L_2]} \\ &\times \begin{Bmatrix} 1 & J_2 & J_1 \\ 0 & l_1 & l_2 \end{Bmatrix} \begin{Bmatrix} L_1 & J_1 & S_2 \\ J_2 & L_2 & 1 \end{Bmatrix}, \end{aligned} \quad (\text{A5})$$

where  $[J] = (2J + 1)$  and  $d_{M, \mu}^{(1)}(\theta)$  are Wigner functions. The angular dependence in Eq. (A4) can be expressed as a linear combination of Legendre polynomials  $P_0(\cos \theta)$ ,  $P_2(\cos \theta)$  and  $P_4(\cos \theta)$ . Finally, the  $C_6$  coefficients can be extracted from this expression according to  $\delta E_{\text{vdW}} = -C_6/R^6$ .

For the vdW interaction between two atoms in the  $5snp(^1P_{1,x})$  states, the general expression (A4) can be broken into contributions from the three dominant channels: (1)  $nP + nP \rightarrow n'S + n''S$ , (2)  $nP + nP \rightarrow n'D + n''D$  and (3)  $nP + nP \rightarrow n'S + n''D$ . Denoting the angular factors inside the closed brackets in Eq. (A4) with functions  $f_{ss}(\theta)$ ,  $f_{dd}(\theta)$  and  $f_{sd}(\theta)$ , we can express (A4) as

$$\delta E_{\text{vdW}} = -\frac{1}{R^6} (f_{ss}(\theta) S_{ss} + f_{dd}(\theta) S_{dd} + f_{sd}(\theta) S_{sd}), \quad (\text{A6})$$

where the reduced sums  $S_{ss}$ ,  $S_{ss}$  and  $S_{ss}$  are defined in Eq. (8).

- 
- [1] E. Urban, T. A. Johnson, T. Henage, L. Isenhower, D. D. Yavuz, T. G. Walker, and M. Saffman, Nat. Phys. **5**, 110 (2009), ISSN 1745-2473, URL <http://www.nature.com/doi/10.1038/nphys1178>.
- [2] A. Gaëtan, Y. Miroshnychenko, T. Wilk, A. Chotia, M. Viteau, D. Comparat, P. Pillet, A. Browaeys, and P. Grangier, Nat. Phys. **5**, 115 (2009), ISSN 1745-2473, URL <http://www.nature.com/doi/10.1038/nphys1183>.

- [3] I. I. Beterov, M. Saffman, E. A. Yakshina, V. P. Zhukov, D. B. Tretyakov, V. M. Entin, I. I. Ryabtsev, C. W. Mansell, C. MacCormick, S. Bergamini, et al., Physical Review A **88**, 010303 (2013), ISSN 1050-2947, URL <http://link.aps.org/doi/10.1103/PhysRevA.88.010303>.
- [4] M. Saffman, T. Walker, and K. Mølmer, Rev. Mod. Phys. **82**, 2313 (2010), ISSN 0034-6861, URL <http://link.aps.org/doi/10.1103/RevModPhys.82.2313>.

- [5] D. Jaksch, J. Cirac, P. Zoller, S. Rolston, R. Côte, and M. Lukin, *Phys. Rev. Lett.* **85**, 2208 (2000), ISSN 1079-7114, URL <http://www.ncbi.nlm.nih.gov/pubmed/10970499>.
- [6] M. Müller, I. Lesanovsky, H. Weimer, H. P. Büchler, and P. Zoller, *Phys. Rev. Lett.* **102**, 170502 (2009), URL <http://link.aps.org/doi/10.1103/PhysRevLett.102.170502>.
- [7] H. Weimer, M. Müller, I. Lesanovsky, P. Zoller, and H. P. Büchler, *Phys. Rev. Lett.* **6**, 382 (2010).
- [8] T. Pohl, E. Demler, and M. D. Lukin, *Phys. Rev. Lett.* **104**, 043002 (2010), URL <http://link.aps.org/doi/10.1103/PhysRevLett.104.043002>.
- [9] F. Cinti, P. Jain, M. Boninsegni, A. Micheli, P. Zoller, and G. Pupillo, *Phys. Rev. Lett.* **105**, 135301 (2010), URL <http://link.aps.org/doi/10.1103/PhysRevLett.105.135301>.
- [10] M. Saffman and K. Mølmer, *Physical Review Letters* **102**, 240502 (2009), ISSN 0031-9007, URL <http://link.aps.org/doi/10.1103/PhysRevLett.102.240502>.
- [11] T. Peyronel, O. Firstenberg, Q.-Y. Liang, S. Hofferberth, A. V. Gorshkov, T. Pohl, M. D. Lukin, and V. Vuletić, *Nature* **488**, 57 (2012).
- [12] D. E. Chang, V. Vuletić, and M. D. Lukin, *Nature Photonics* **8**, 685 (2014).
- [13] M. Saffman and K. Mølmer, *Physical Review A* **78**, 012336 (2008), ISSN 1050-2947, URL <http://link.aps.org/doi/10.1103/PhysRevA.78.012336>.
- [14] R. Mukherjee, J. Millen, R. Nath, M. P. A. Jones, and T. Pohl, *Journal of Physics B: Atomic, Molecular and Optical Physics* **44**, 184010 (2011), ISSN 0953-4075, URL <http://stacks.iop.org/0953-4075/44/i=18/a=184010?key=crossref.48c64b3448df32d721e72d6d551bc6ab>.
- [15] T. Topcu and A. Derevianko, *Phys. Rev. A* **89**, 023411 (2014), URL <http://link.aps.org/doi/10.1103/PhysRevA.89.023411>.
- [16] X. Xu, T. H. Loftus, J. L. Hall, A. Gallagher, and Y. J., *J. Opt. Soc. Am. B* **20**, 968 (2003).
- [17] U. D. Rapol, A. Krishna, A. Wasan, and N. V., *Eur. Phys. J. D* **29**, 409 (2004).
- [18] B. Hemmerling, G. K. Drayna, E. Chae, A. Ravi, and D. J. M., *New J. Phys.* **16**, 063070 (2014).
- [19] F. Sorrentino, G. Ferrari, N. Poli, R. Drullinger, and T. G. M., *Mod. Phys. Lett.* **20**, 1287 (2006).
- [20] T. F. Gallagher, *Rydberg Atoms* pp. Cambridge Monographs on Atomic, Molecular and Chemical Physics (1994).
- [21] C. L. Vaillant, M. P. A. Jones, and R. M. Potvliege, *Journal of Physics B: Atomic, Molecular and Optical Physics* **47**, 155001 (2014), URL <http://stacks.iop.org/0953-4075/47/i=15/a=155001>.
- [22] B. J. Bloom, T. L. Nicholson, J. R. Williams, S. L. Campbell, M. Bishof, X. Zhang, W. Zhang, S. L. Bromley, and J. Ye, *Nature* **506**, 71 (2014), ISSN 1476-4687, URL <http://www.ncbi.nlm.nih.gov/pubmed/24463513>.
- [23] N. Hinkley, J. a. Sherman, N. B. Phillips, M. Schioppo, N. D. Lemke, K. Beloy, M. Pizzocaro, C. W. Oates, and a. D. Ludlow, *Science (New York, N.Y.)* **341**, 1215 (2013), ISSN 1095-9203, URL <http://www.ncbi.nlm.nih.gov/pubmed/23970562>.
- [24] A. D. Ludlow, M. M. Boyd, J. Je, E. Peik, and P. Schmidt, *arXiv:1407.3493v1* pp. 1–90 (2014), URL <http://arxiv.org/abs/1401.2378>.
- [25] V. K. K. D. A. Varshalovich, A. N. Moskalev, *World Scientific*, 1989 (1989).
- [26] J. Millen, Durham University (PhD Thesis) **PhD Thesis**, <http://etheses.dur.ac.uk/849/> (2011).
- [27] P. Esherick, *Physical Review A* **15** (1977), URL [http://pra.aps.org/abstract/PRA/v15/i5/p1920\\_1](http://pra.aps.org/abstract/PRA/v15/i5/p1920_1).
- [28] D. F. Beigang, R., K. Lucke, A. Timmerman, P.J. West, *Optics Communications* **42**, 19 (1982).
- [29] C. L. Vaillant, M. P. A. Jones, and R. M. Potvliege, *Journal of Physics B: Atomic, Molecular and Optical Physics* **45**, 135004 (2012), ISSN 0953-4075, URL <http://stacks.iop.org/0953-4075/45/i=13/a=135004?key=crossref.313be1041e0e03b93c6c39a65a2b6274>.
- [30] J. E. Sansonetti and G. Nave, *Journal of Physical and Chemical Reference Data* **39**, 033103 (2010), ISSN 00472689, URL <http://link.aip.org/link/JPCRBU/v39/i3/p033103/s1&Agg=doi>.
- [31] W. R. Johnson, D. R. Plante, and J. Sapirstein, *Advances In Atomic, Molecular, and Optical Physics* **35**, 255 (1995).